Development, characterisation and cytotoxicity studies of erlotinib entrapped gellan gum nanoparticles

Soumiya Sukumar, Santhiagu Arockiasamy* and Manjusha Chemmattu Moothona

School of Biotechnology,
National Institute of Technology Calicut,
Calicut, Kerala 673601, India
Email: soumiyas15@gmail.com
Email: asanthiagu@nitc.ac.in
Email: manjuabijith@gmail.com
*Corresponding author

Abstract: Gellan gum is an anionic, water-soluble polysaccharide produced by the bacterium *Sphingomonas paucimobilis* ATCC 31461 via the fermentation process. The gellan gum-erlotinib (GgE) nanoparticles were synthesised by the emulsion cross-linking method. The synthesised GgE nanoparticles were characterised by scanning electron microscopy (SEM), Fourier transform infrared spectroscopy (FTIR), X-ray diffraction (XRD), differential scanning calorimetry (DSC), thermogravimetric (TGA), particle size and zeta potential analysis. The influence of gellan, drug and calcium chloride concentration on drug loading and entrapment efficiency was evaluated. *In-vitro* release behaviour' of erlotinib was examined by dialysis bag technique. Further, to assess the potential anticancer efficacy of GgE nanoparticles, *in-vitro* cytotoxicity studies on HepG2 cell lines by SRB assay were carried out. SEM results showed spherical smooth-surfaced nanoparticles. FTIR confirmed the interaction between polymer matrix and erlotinib. The drug loading and entrapment efficiency of GgE nanoparticles increased with gellan and drug concentration. The GgE nanoparticles showed pH-responsive drug release leading to faster release of erlotinib at acidic buffer than neutral and alkaline. The GgE nanoparticles exhibited a cytotoxic effect on HepG2 cells and their cytotoxicity was more significant than free erlotinib and gellan gum.

Keywords: gellan gum; erlotinib; *Sphingomonas paucimobilis*; GgE nanoparticles; *in-vitro* drug release; cytotoxicity.

Biographical notes: Soumiya Sukumar is pursuing her PhD in the School of Biotechnology at NIT Calicut. She received her MTech in Biotechnology from St Joseph's College of Engineering, Chennai. Her area of interest is bioprocess technology, nanotechnology, bioremediation and molecular biology.

Santhiagu Arockiasamy is a Professor in the School of Biotechnology at NIT Calicut. He received his PhD in Biochemical Engineering from Banaras Hindu University, Varanasi. His areas of interest include modelling and simulation of bioprocesses, microbial production of biopolymers and nanobiotechnology.

Manjusha Chemmattu Moothona is a research scholar in the School of Biotechnology at NIT Calicut. She received her MSc in Microbiology from Calicut University. Her area of interest is microbiology, bioprocess technology, nanotechnology and molecular biology.

1   Introduction

The critical environmental problems, including the growing challenges of waste disposal and the threat of global warming caused by several polymers non biodegradability, have raised attention worldwide. Therefore, the application of biodegradable polymer as an alternative to non-biodegradable polymers has been evoking significant interest recently. Current trends in biodegradable polymers exhibit substantial progress in novel design strategies and engineering to render advanced polymers with comparably more excellent performance.

The biopolymer gellan gum is produced by *Sphingomonas paucimobilis* ATCC 31461 via the fermentation process. *Sphingomonas* is a genus of gram-negative, chemoheterotrophic, aerobic, rod-shaped bacteria. Gellan gum is an anionic, water-soluble exopolysaccharide composed of glucose, rhamnose and glucuronic units. The gellan gum biosynthetic pathway can be divided into the following parts: synthesis of sugar-activated precursors, assembly of tetrasaccharide repeat units attached to an inner membrane, transport of the repeat units to the periplasmic space, polymerisation of the tetrasaccharide repeat units and their export through the outer membrane (Bajaj et al., 2007).

The gellan gum is a compound with high-molecular-weight and water holding capacity. It has diverse industrial applications due to rheological characteristics. Gene therapy, tissue engineering, regenerative medicine, implantable devices, novel drug delivery systems, etc., are some of the arenas where gellan polymer is widely used. Biodegradable polymer finds application in a controlled drug release system due to their reabsorbing ability by the body (Heller and Domb, 2003).

There has been substantial interest in producing biodegradable nanoparticles as useful drug delivery methods in the last decades. Biodegradable polymeric nanoparticles are submicron-sized particles prepared using natural or synthetic polymers (Mahapatro and Singh, 2011). Such nanoparticles encapsulate therapeutic agents within their polymeric matrix. They are highly preferred due to delivering the drug to a target site, enhancing the therapeutic benefit and minimising side effects. Some of the advantages of biodegradable polymeric nanoparticles are non-toxic, noninflammatory, stability in blood, biocompatibility with tissue and cell, biodegradability, sustained drug release and suitable delivery of various molecules such as drugs, peptides and proteins (Sharma et al., 2016).

Natural macromolecules such as gellan gum and chitosan are suitable polymers to prepare polymeric nanoparticles. Various analytical techniques have been used to synthesise the polymeric nanoparticle based on the application and nature of drugs to be encapsulated (Sailaja et al., 2011).

There are several techniques available to examine physicochemical states and drug excipient interaction. The most commonly used methods are XRD, FTIR, DSC, etc. Particle size and size distribution are essential characteristics of nanoparticles that

influence drug loading, drug release and nanoparticle stability (Panyam and Labhasetwar, 2003).

The drug encapsulation efficiency of polymeric nanoparticles is higher when the therapeutic agents are incorporated at the time of nanoparticle production (Soppimath et al., 2001). The polymeric nanoparticle drug delivery system with a high loading capacity lower the quantity of the carrier required for administration and is considered successful (Singh and Lillard, 2009). Encapsulation efficiency and drug loading depend on the solubility of the drug in the excipient matrix, i.e., associated with the molecular weight, matrix composition, drug-polymer interactions and end functional groups ester or carboxyl in the drug or matrix (Govender et al., 1999).

Understanding the release mechanisms and parameters that influence drug release is vital to modify drug release. The release rates of polymeric nanoparticles are linked with the following process: desorption of the adsorbed drug, nanoparticle matrix erosion, diffusion through the nanoparticle matrix and a combined erosion-diffusion. The *in-vitro* drug release profile of the polymeric nanoparticles is carried out using side-by-side diffusion cells with biological membranes, dialysis bag diffusion, reverse dialysis sac and ultrafiltration method. The *in-vitro* drug release rate depends on nanoparticle size, loading efficiency of the drug, biodegradation, diffusion and solubility of the matrix material (Gültekin and Değim, 2013).

Cancer is an ever-increasing threat and research continues for more judicious therapies that destroy tumor cells without harming normal tissues. The polymeric nanoparticles can deliver therapeutic agents to tumor cells with greater efficiency and reduced cytotoxicity on the surrounding healthy tissues. There are various assays used for the assessment of nanoparticle cytotoxicity. Sulforhodamine B (SRB) assay assesses *in-vitro* toxicity of nanoparticles in cancer cell lines (Kumar et al., 2012).

In the present study, the emulsion cross-linking method was used to synthesise gellan gum erlotinib nanoparticles. The polymeric nanoparticles were characterised by SEM, FTIR, XRD, TGA, DSC, particle size and zeta potential. The drug loading and entrapment efficiency of erlotinib-loaded gellan gum nanoparticles were elucidated. *In-vitro* release studies were performed using the dialysis bag technique. HepG2 cells were used for *in-vitro* cell line experiments. The anticancer effect of GgE nanoparticles (NPs), free erlotinib and gellan were investigated using SRB assay and IC_{50} was analysed.

2 Materials and methods

2.1 Materials

The materials for the synthesis of GgE NPs include calcium chloride, dioctyl sulfosuccinate, methylene chloride and DMSO , which were purchased from Sigma-Aldrich (USA). Poly vinyl alcohol and hydrochloric acid (HCl) were procured from Merck (Germany). Erlotinib was obtained from Regional Cancer Centre (Trivandrum, India) as a gift sample. The materials for cytotoxicity studies Dulbecco's modified Eagle medium (DMEM), fetal bovine serum (FBS), penicillin and streptomycin were purchased from Sigma-Aldrich (USA). The HepG2 cell line used in the study was obtained from the National Centre for Cell Science (Pune, India). All aqueous solutions were prepared by

utilising double-distilled water. All the chemicals used were of analytic grade and without any further purification.

The gene gelD encoding the protein for polymerisation and export of gellan from strain *Sphingomonas paucimobilis* ATCC 31461 was extracted, amplified by polymerase chain reaction (PCR) and cloned in pBBR122 vector. The nucleotide sequence was submitted in GenBank under accession number – MK430034. The recombinant plasmid pBBR122-gelD was transformed into *Sphingomonas paucimobilis* ATCC 31461 by electroporation technique. Then the recombinant protein was purified using affinity chromatography employing Ni-nitrilotriacetate (Ni-NTA) agarose column (Soumiya et al., 2021).

2.2   Microorganism

The recombinant *Sphingomonas paucimobilis* ATCC 31461 grown in YPG medium (glucose 20 g/l; peptone 5 g/l; yeast extract 3 g/l; NaCl 5 g/l and agar 20 g/l) was used as slant culture. The YPG agar slants were incubated for 48 h at 30°C. The slants were stored at 4°C and subcultured periodically.

2.3   Inoculum

One-two loop full of recombinant *Sphingomonas paucimobilis* ATCC 31461 culture from the agar slant was inoculated into a 250 ml Erlenmeyer flask containing 50 ml of YPG medium. The flasks were then incubated for 24 h at 30°C on an orbital shaker at 200 rpm.

2.4   Gellan gum production in 6-L- stirred type fermenter

The 6 l stirred type fermenter with a working volume of 4 l of production medium (YPG) was inoculated with 24 h old standard inoculum. The culture broth was maintained at a pH (6.5) and cultivated for 48 h at 30°C with 500 rpm and 100% dissolved oxygen.

2.5   Extraction of gellan gum

After fermentation, the fermented broth obtained was immersed in a boiling water bath for 15 min and cooled. The pH of the heated broth was maintained at 10 by the addition of NaOH. The broth was again heated for 10 min at 80°C, cooled and the broth pH was lowered to 7.0 by adding 2 M HCl. The fermentation broth was then centrifuged at 8,000 rpm for 30 min at 4°C to separate the cells. Dimethyl sulfoxide (DMSO) was incorporated into the cells to remove the adhered polymer. The DMSO-treated cells were centrifuged at 8,000 rpm for 30 min at 4°C and the resultant supernatant was collected. Three volumes of ice-cold isopropanol were mixed with supernatant, stirred vigorously and incubated overnight at 4°C for precipitation of the polymer. The resultant precipitate was centrifuged at 8,000 rpm for 30 min at 4°C. The precipitate (polymer) collected was dried at 80°C for 12 h in a hot air oven (Fialho et al., 1999).

2.6   High-performance liquid chromatography

The monosaccharide composition of gellan gum was determined using an HPLC (Shimadzu). The injection volume was 20 µl. The exopolysaccharides were determined with an RI detector.

2.7   Nuclear magnetic resonance

The ^{1}H NMR spectra were recorded using a Bruker spectrometer. Chemical shifts were expressed in ppm using D_2O as an internal standard. The data were acquired and processed employing Bruker software.

2.8   Preparation of Gellan gum-erlotinib nanoparticles

The emulsion cross-linking method was used for the synthesis of the GgE nanoparticles. A set of preparatory studies was carried out to identify the appropriate drug and gellan gum concentration needed to attain stable nanoparticles. For GgE nanoparticle preparation, 0.2–2.4 % w/v of gellan gum was dissolved in distilled water by heating at 95°C for 15 minutes with vigorous stirring to form solution-I. 0.2–2.4% w/v of erlotinib was dissolved in distilled water with continuous stirring to form solution-II. One ml of solution I and solution II were added to the AOT solution in methylene chloride (10% w/v) while under sonication. The reaction mixture was sonicated employing a probe-type sonicator in an ice bath at a pulse mode of 21% amplitude for 5 min. To this solution, 3.5% of polyvinyl alcohol was added under sonication at pulse mode of amplitude 21% for 3 min in an ice bath. 60% of an aqueous solution of calcium chloride was added to the above solution under magnetic stirring. The solution was agitated at room temperature overnight in a closed round bottom flask. The methylene chloride was dissipated from the solution by using a rotary vacuum evaporator. The nanoparticle-containing solution was then centrifuged at 12,000 rpm for 25 min. The precipitate thus obtained was washed extensively with double distilled water followed by ultracentrifugation to remove any polyvinyl alcohol and unentrapped drug. The resultant pellet was resuspended in water and lyophilised (Mahesh et al., 2007).

2.9   Sample characterisation

2.9.1   Scanning electron microscopy

The SEM studies were performed to examine the surface morphological characteristics. The scanning electron micrographs of the GgE nanoparticles were taken by the SEM microscope. The SEM instrument used was (Hitachi SU6600) operated at an accelerating voltage of 20 kV. The electrons were emitted via Schottky field emission electron source and condenser lenses focused the resultant electron beam. The interaction between the electron beam and constituent atoms of the sample produced secondary electrons detected by Everhart – Thornly detector. After detecting secondary electrons, electronic signals produced were amplified, processed and translated into images. The samples were imaged at a working distance of about 11 mm and magnification at 100 µm.

2.9.2   Fourier transform infrared spectroscopy

The fourier transform infrared analysis was carried out for gellan gum, pure drug (erlotinib) and Gellan gum erlotinib (GgE) nanoparticles using FTIR spectrophotometer Agilent Technologies model Cary 630. The information about the functional group present in the samples was determined using FTIR spectroscopy based on the infrared regions band values. The FTIR spectrophotometer was operated in the spectral window from 4,000 to 400 cm^{-1} scanning range, resolution of 8cm^{-1} and a sample scan of 32. The detector DTGS and Transmission accessory were used to record the FTIR spectra. The spectra of the samples were acquired and processed with the aid of MicrolabPro software.

2.9.3   X-ray diffraction

XRD pattern of gellan, erlotinib and GgE nanoparticle was obtained using an X-ray diffractometer (Bruker D8 Advance). The instrument was run at a voltage of 40 kV and a current of 40 mA at room temperature. The data collection has been made at a step time of 57.60 s and the continuous scan mode. The scattering angle ranged from 3° to 80° of 2θ.

2.9.4   Thermogravimetric analysis

Hitachi STA7,300 was used to estimate the thermal weight loss of the synthesised GgE nanoparticles. The temperature was programmed to 750°C at a heating rate of 20°C/min in a nitrogen atmosphere.

2.9.5   Differential scanning calorimetry

DSC technique was used to identify the thermal behaviour' or physical state of the erlotinib inside the GgE nanoparticles employing a differential scanning calorimeter (Netzsch DSC 204 F1). The sample was operated at a heating rate of 20°C/min over a temperature range of 20° C–300°C under a nitrogen atmosphere.

2.9.6   Particle size analysis

The mean particle size and size distribution study of GgE nanoparticles were carried out by dynamic light scattering using a Malvern Zetasizer Ver.7.13. The particle size measurement was performed at a scattering angle of 90° at a temperature 25°C. The diameter was averaged from three independent experiments and expressed as mean ± standard deviation.

2.9.7   Zeta potential measurement

Zeta potential estimates the surface charge and stability of nanoparticles. Zeta potential of GgE nanoparticles was performed in a Malvern Zetasizer Ver.7.13. The measurements were conducted at 25°C using a solution of the nanoparticles dispersed in distilled water. The results (mean ± SD) were averaged from three independent experiments.

2.9.8   Drug content estimation

The drug content of the GgE nanoparticle was estimated by weighing 100 mg nanoparticle and dissolving in phosphate buffer (100 ml) of pH 6.8 under magnetic stirring at room temperature. The sample was then filtered through a 0.45 μ membrane filter. After filtration, erlotinib content in the nanoparticle sample was measured in a UV-VIS spectrophotometer (Lambda 25, Perkin Elmer, Germany) at 285 nm (Nagarajan et al., 2015). The percentage of drug loading was calculated as follows:

$$Drug\ content\ (mg) = Weight\ of\ drug\ in\ nanoparticles\ /\ Weight\ of\ nanoparticles\ *100$$

2.9.9   Determination of entrapment efficiency

The centrifugation method was adapted to determine the entrapment efficiency of the GgE nanoparticle. The drug-loaded nanoparticle was centrifuged at 4,000 rpm for 30 min at 4ºC. The clear supernatant collected after centrifugation was filtered using a 0.45 μ membrane filter. Finally, the filtered solution was analysed on a UV visible spectrophotometer at 285 nm against phosphate buffer pH 6.8 as blank (Das et al., 2005). The following formula measured the entrapment efficiency:

$$EE\% = Amount\ of\ drug\ present\ /\ Theoretical\ drug\ load\ expected\ *100$$

The amount of drug loaded and entrapment efficiency of erlotinib-loaded gellan gum nanoparticles was determined by studying the effect of the following parameters (Table 1).

Table 1   Parameters and its concentration for determination of optimum drug loading and entrapment efficiency

Parameters	Concentration
Drug	0.2–2.4 % w/v
Gellan gum	0.2–2.4% w/v
Calcium chloride	0.1M–1.0M

2.10   In-vitro drug release studies

The *in-vitro* drug release of the GgE nanoparticle was performed using the dialysis bag method. The dialysis tubing of a molecular weight cut-off range of 12,000–14,000 was used. Dialysis tubing was immersed in a 2% sodium bicarbonate solution and 1 mM of EDTA (pH 8). The tubing was then boiled in distilled water for 10 min. After boiling, tubing was cooled, transferred to ethanol solution to prevent microbial growth. The dialysis tubing was then stored at 4ºC. The dialysis tubing was thoroughly rinsed with distilled water before usage. Three dissolution medium citrate, carbonate bicarbonate and phosphate buffer with pH 4.8, 10.2 and 7 were sequentially used to study the *in-vitro* drug release pattern. 10 mg of GgE nanoparticle was placed on the dialysis bag, tied at both ends and suspended in a beaker containing 200 ml of the dissolution medium. The beaker was then kept in a magnetic stirrer maintained at 37ºC and stirred at 100 rpm for 1 h and 6 h. 2 ml of the sample were withdrawn at regular intervals (8–63 min) and restored with an equivalent amount of the fresh dissolution medium. The samples were

then filtered employing a 0.45 μ membrane filter and the percentage drug release was assayed at 285 nm by UV absorption spectroscopy (Jeong et al., 2010).

2.11   Determination of cellular cytotoxicity by Sulforhodamine B (SRB) assay

The cytotoxicity of gellan gum (Gg), erlotinib (E) and gellan gum – erlotinib (GgE) nanoparticles against the Human hepatocellular carcinoma (HepG2) cell line was measured using Sulforhodamine B (SRB) assay. The HepG2 cells were cultured in DMEM high glucose medium supplemented with 10% fetal bovine serum and antibiotics penicillin (100 units/ml) and streptomycin (100 μg/ml). The cell density of 0.5×10^5 cells/ml was seeded in a 96-well microtiter plate. After inoculation of cells, the microtiter plates were maintained at 37°C for 24 h under a 5% CO_2, humidified atmosphere of 95% air for cell adherence before the addition of formulations (Gg, E and GgE NPs). The cells were then treated with samples Gg, E and GgE NPs of different concentrations (5, 10, 20, 40, 80 and 100 μM). The plates were incubated for 48 h following sample addition. The cells were fixed by adding ice-cold 1% trichloroacetic acid (TCA) and incubated at 4°C for 1 h. The supernatant was then discarded, plates were washed using distilled water and air-dried. 0.4% SRB solution dissolved in 1% acetic acid was added to each of the wells and the plates were stored at room temperature for 30 min. The unbound SRB was removed off the plate by washing 5 times using 1% acetic acid followed by air drying. 10 mM tris-base solution was added to each well to solubilise the bound SRB and the plates were shaken for 10 min. The absorbance was estimated at a wavelength of 540 nm using a microplate reader (Skehan et al., 1990).

3   Results and discussion

3.1   Isolation of gellan gum

After 48 h of fermentation, recombinant *S paucimobilis* produced gellan gum polymer in YPG containing medium under optimised conditions.

3.2   HPLC

The estimation of the monomer content of gellan gum by HPLC is depicted in Figure 1. Gellan gum produced by recombinant *Sphingomonas paucimobilis* was composed mainly of glucose, rhamnose and glucuronic acid. In terms of peak area, glucose (58%) is the dominant monosaccharide, whereas glucuronic acid (19%) and rhamnose (15%) were observed in minor levels.

3.3   NMR

Figure 2 depicts the ^{1}H NMR spectra of gellan gum. The spectrum of gellan showed peaks at 1.20–1.30 ppm attributed to –CH₃ of rhamnose. The peaks at 3.2–4.6 ppm correspond to –CH- of glucose, glucuronic acid and rhamnose.CH of glycosidic bonds in sugars were observed at peak 5.1–5.2 ppm. The peaks at 5.2 and 5.1 ppm were ascribed to the H of C1 with glucoside bonds of glucuronic acid and glucose (Lu et al., 2019).

Figure 1 HPLC chromatogram of gellan gum
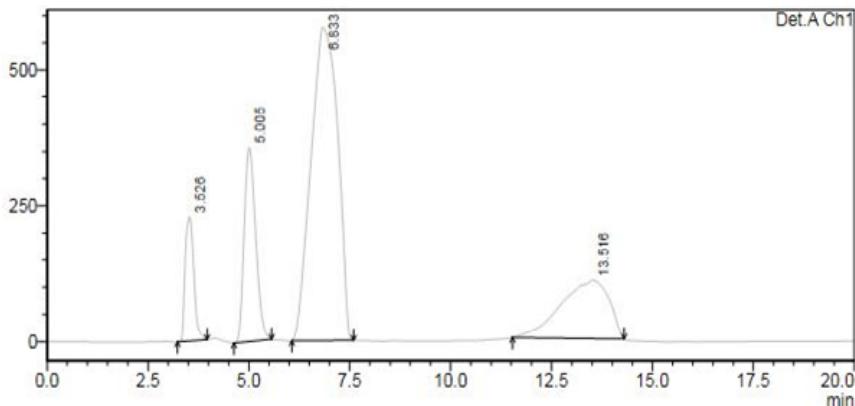
Figure 2 ^{1}H NMR spectrum of gellan gum
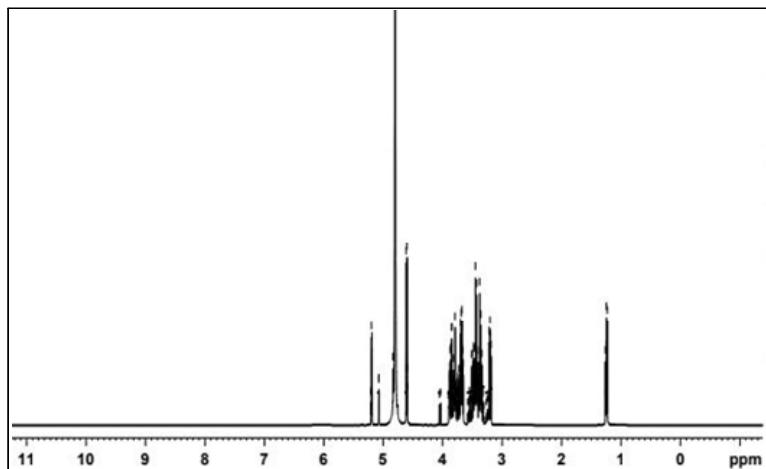
3.4 Synthesis of GgE NPs

The GgE nanoparticles were prepared by emulsion cross-linking method using AOT as the surfactant, PVA as the emulsifier and calcium ions as cross-linker. Gellan forms insoluble gels on the addition of calcium ions. Di-octyl sodium sulfosuccinate or AOT comprises a sulfonic group in its polar sulfosuccinate head with a significant branching hydrocarbon tail. Due to its double chain amphiphilic nature, AOT forms a bilayer structure in multiple emulsions. AOT forms reverse micelles in non-polar solvents like methylene chloride.AOT interacts with calcium ions to form insoluble salts. The aqueous core of the gellan was entrapped in the reverse micelles produced by the AOT in methylene chloride and was further emulsified in the aqueous phase employing PVA as a secondary emulsifier. Based on the above characteristic and the emulsion method applied, nanoparticles are expected to have a calcium-crosslinked core composed of

gellan and AOT head groups encompassed by a hydrophobic matrix constituting an AOT side chain with erlotinib encapsulated in the core (Varsha et al., 2015).

3.5   Characterisation

3.5.1   Morphological studies

The SEM method was used to reveal the morphological features. Figure 3(a) depicts the SEM image for gellan gum. The SEM micrographs showed that the gellan exhibited a smooth and porous surface. Figure 3(b) shows the SEM image of the GgE nanoparticles. The nanoparticle surface showed a smooth texture and morphology related to a spherical shape (Dhar et al., 2012).

Figure 3   SEM of (a) gellan (b) GgE nanoparticles

(a)

(b)
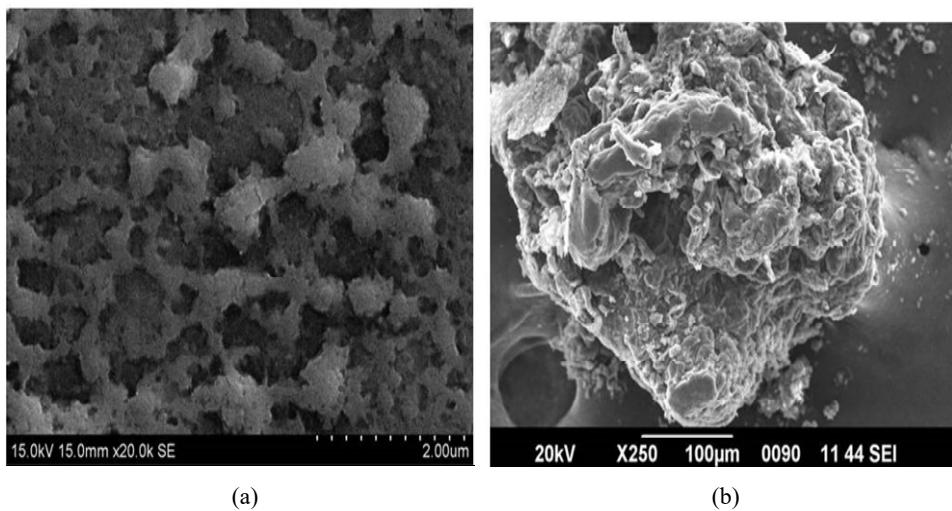
3.5.2   FTIR for GgE nanoparticles

The drug-polymer interaction was determined using FTIR analysis. From the FTIR spectrum, various functional groups present in the sample were examined. The peak at $2,885.0 cm^{-1}$ is attributed to the C-H stretching of gellan gum. $1,599.0 cm^{-1}$ and $1,401.5 cm^{-1}$ corresponds to C = C stretching. The spectra showed a strong absorption peak at $3,309.9 cm^{-1}$ attributed to the stretching vibration of OH. The band at $1,017.6 cm^{-1}$ corresponds to C-F stretching for alky halide. The band at $2,113.4 cm^{-1}$ is assigned to C ≡ C stretching. O = C-O-C stretching is observed at $1,297.1 cm^{-1}$. The band at $808.1 cm^{-1}$ is attributed to = C-H bending Figure 4(a).

While in the case of erlotinib, the band around $3,328.5 cm^{-1}$ and $3,272.6 cm^{-1}$ corresponds to the stretching of the O-H bond of alcohol. The peak near $2,855.1 cm^{-1}$ and $3,015.4 cm^{-1}$ are assigned to C-H stretching. The band in the region $1,632.6 cm^{-1}$ can be assigned to the NH bending of amines. The band at $1,744.4 cm^{-1}$ corresponds to the C = O bond stretch. The bands at $1,021.3 cm^{-1}$ and $943.0 cm^{-1}$ are attributed to = C-O-C symmetric and asymmetric stretching and = C-H bending respectively. The band at $779.0 cm^{-1}$ corresponds to the C-Cl stretch. The band at $2,109.7 cm^{-1}$ is due to the

presence of C ≡ C stretching. The peak near 2,683.7cm⁻¹ and 2,918.5cm⁻¹ correspond to O-H stretching. The band 1,572.9cm⁻¹ is developed for C = C stretching Figure 4(b).

Figure 4 FTIR spectrum of (a) gellan gum (b) erlotinib (c) GgE nanoparticles (see online version for colours)
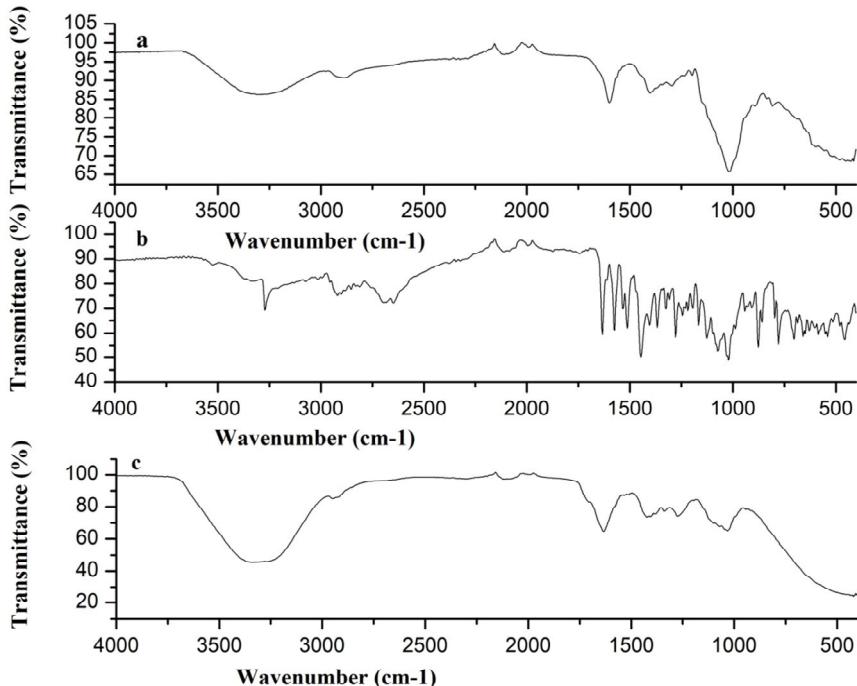
In GgE NPs, the broad absorbance at 3,339.7cm⁻¹ corresponds to the stretching vibration of OH. The peaks in the range of 2,113.4cm⁻¹ are associated with the stretching of C ≡ C. 1,032.5cm⁻¹and 1,338.1cm⁻¹ is attributed to the stretching mode of C-F. 1,274.7cm⁻¹ represents the = C-O-C symmetric and asymmetric stretching. The band present at 1,632.6cm⁻¹ is assigned to the N-H bending. The stretch band of C-I is observed at 4,21.2cm⁻¹ Figure 4(c).

Any shifting or disappearance of the FTIR absorption bands implies the interaction between the drug and the polymer (Singh et al., 2018). By comparing the FTIR spectra of gellan gum and GgE NPs, it was observed that the disappearance of the peak occurred at 2,885.0 cm⁻¹ in GgE NPs corresponding to C-H stretching. It was observed that the bands corresponding to OH stretching in gellan gum were shifted from 3,309.9 cm⁻¹ to 3,339.7cm⁻¹ in GgE NPs. The bands at 1,632.6cm⁻¹ for the drug were also observed in nanoparticles, indicating the chemical stability of erlotinib on the surface of nanoparticles. The erlotinib characteristic peaks at 2,109.7cm⁻¹ attributed to C ≡ C stretching were shifted to 2,113.4cm⁻¹ in GgE NPs also confirmed the interaction of the polymer with the drug. These results indicated erlotinib was successfully loaded onto the gellan gum nanoparticles (Unsoy et al., 2014).

3.5.3   X-ray diffraction

X-ray diffractometry examines the physical nature of drugs in the polymer matrix, as it renders useful information on drug release mechanisms and dynamics. Few drugs are dispersed in the particles in the amorphous phase. In contrast, other drugs are loaded in the crystalline phase based on their characteristics and interactions between drugs and polymers. The diffraction patterns of pure erlotinib, gellan gum and GgE nanoparticle are depicted in Figure 5(a), 5(b) and 5(c) respectively. The diffractogram of erlotinib exhibited intense diffraction peaks at $2\theta = 16°$, $20°$ and $21°$, inferring that it exists in a crystalline state. XRD of the gellan showed a broad peak at a lower diffraction angle (2θ), which exhibits its amorphous nature. Also, peaks were observed at $28°$, $40°$, which indicates the minor crystalline constituent of gellan. In GgE nanoparticles, the diffraction peak intensity was considerably decreased due to the transformation of the erlotinib state from crystalline to amorphous. Due to higher saturation solubility, the amorphous state of the drug in nanoparticles is a beneficial feature compared to the crystalline state. This results in a longer shelf lifetime and durability of the drug in an aqueous medium (Katiyar et al., 2014).

Figure 5   X-ray diffractogarm of (a) erlotinib (b) gellan gum (c) GgE nanoparticles
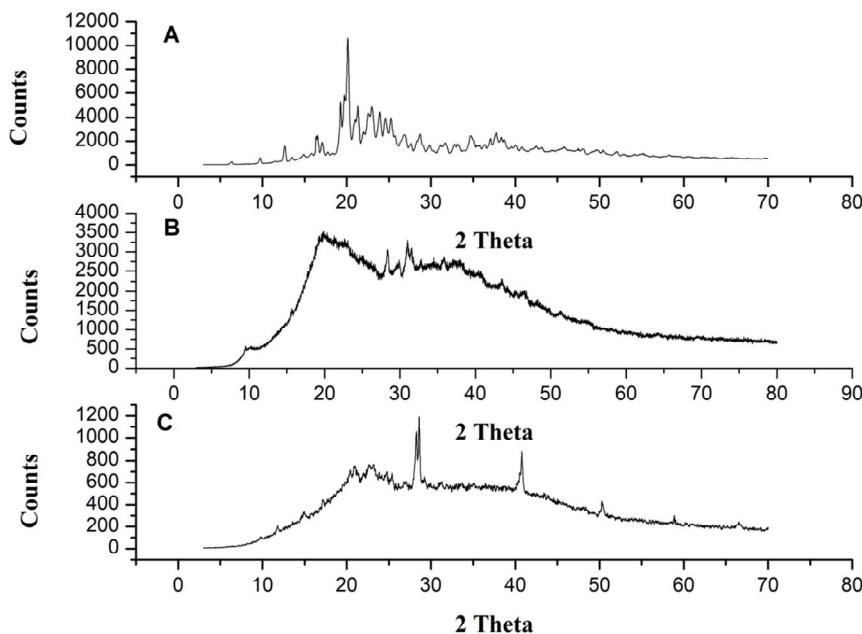
3.5.4   Thermogravimetric analysis

TGA analysis was conducted on the GgE nanoparticles to examine their thermal characteristics. The thermogram of gellan is depicted in Figure 6(a). The gellan starts decomposing after 150°C and mass loss occurred due to loss of free and bound water in the polymer. Further, weight loss was observed at 290°C due to the polymer decomposition. Figure 6(b) presents the thermogram of erlotinib and the weight loss occurred between 250°C and 300°C. Figure 6(c) exhibits the thermal degradation profile

of GgE nanoparticles. The TGA analysis results indicated that the nanoparticles had a significant weight loss step at a higher decomposition temperature around 400°C than gellan gum and drug. Due to the encapsulation of the drug between polymeric chains, the stability of the drug is increased, which leads to a considerable increase in the nanoparticles thermal stability (Güncüm et al., 2018).

Figure 6 TGA curve of (a) gellan gum (b) erlotinib (c) GgE nanoparticles
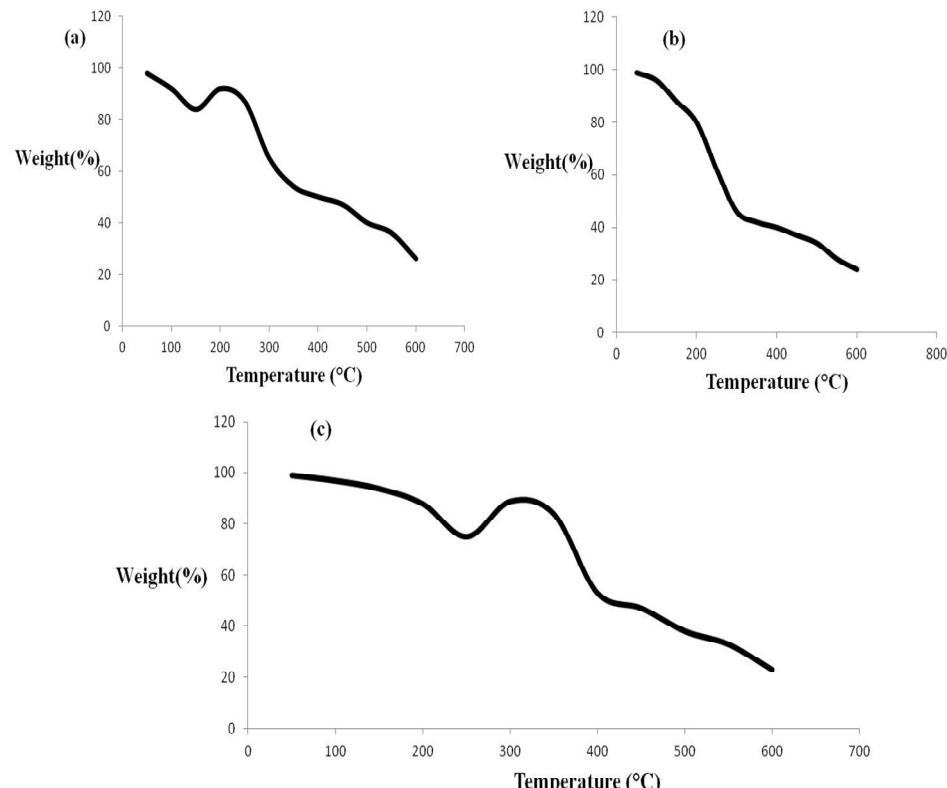
3.5.5 *Differential scanning calorimetry*

The thermogram obtained defines the physical state of polymer and drug in the nanoparticles and helps identify any drug-polymer interactions within the polymeric matrix of the nanoparticles. The DSC thermograms for gellan are shown in Figure 7(a). The appearance of a broad endothermic peak at 26°C is due to the loss of water. The second endothermic peak at around 114°C was also observed. Figure 7(b) depicts the DSC thermogram of the drug. The erlotinib show an endotherm peak at 103°C. Figure 7(c) illustrates the DSC thermogram of GgE nanoparticles. GgE nanoparticles showed peaks at 128.9°C, 195.2°C and minor peaks were observed because of the surfactant presence in little amount in the formulation. At the temperature of 103°C, no peak was observed in the GgE nanoparticle. Therefore, DSC studies revealed no crystalline drug material was present in the nanoparticle sample, which shows the

crystallinity of the drug has been decreased significantly in the nanoparticles. Thus, in the GgE nanoparticle, erlotinib was present in the amorphous state and might be homogeneously dispersed in the gellan gum matrix (Sun et al., 2015).

Figure 7   DSC thermogram of (a) gellan gum (b) erlotinib (c) GgE nanoparticles
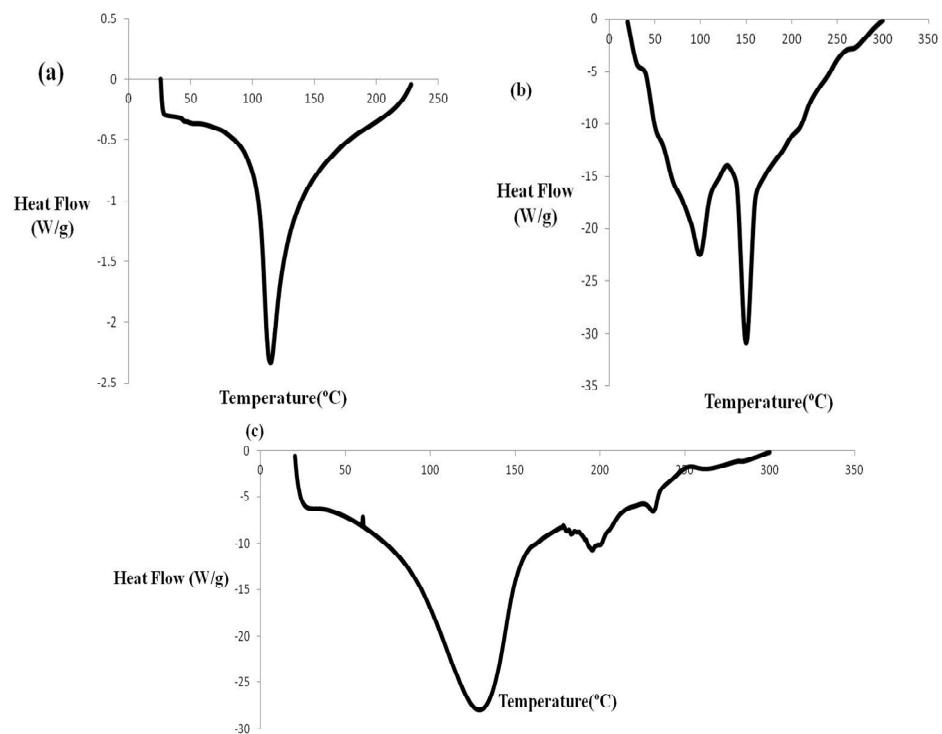
Figure 8   Average particle size and polydispersity index of GgE nanoparticles (see online version for colours)
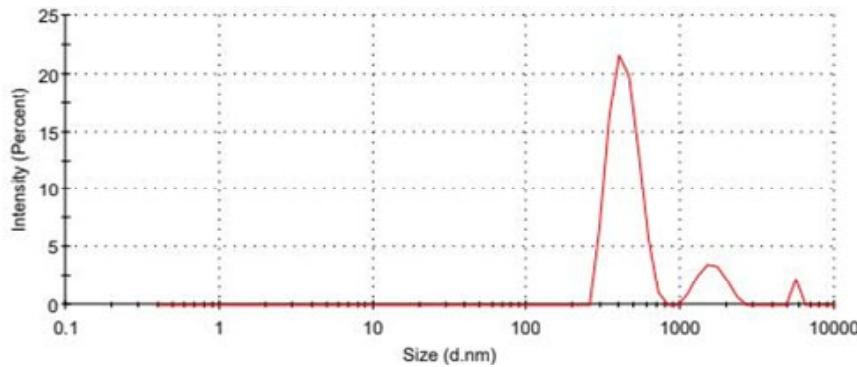
3.5.6 Particle size

The average particle size of the GgE nanoparticle is shown in Figure 8. The average particle size of nanoparticles was 655 nm with polydispersity indices of 0.49, indicating a narrow and favourable particle size distribution (Bera et al., 2020).

3.5.7 Zeta potential

The zeta potential indicates the potential stability of the colloidal system. The zeta potential of the nanoparticle is depicted in Figure 9. The zeta potential (mV) of GgE NPs was found to be –13.9 mV. The higher negative value of zeta potential was obtained for nanoparticle formulation because of carboxyl groups in the polymer (Sun et al., 2015). The zeta potential of GgE NPs showed good stability of the formulation. This might be associated with a surfactant that reduces the electrostatic repulsion between the particles and sterically sustains the nanoparticles by developing a coat around their surface. Also, from the zeta potential estimation, the dominant component on the surface of the particles was predicted as gellan gum. Gellan gum is a negatively charged polymer that confers anionic characteristics to nanoparticles.

Figure 9 Zeta potential of GgE nanoparticles (see online version for colours)
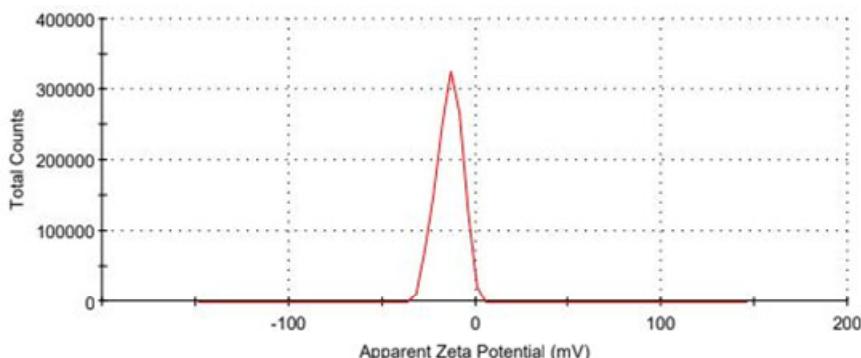
3.5.8 Effect of polymer concentration on drug loading and entrapment efficiency

The effect of drug loading capacity on different concentrations of gellan (0.2%–2.4% w/v) was evaluated. It was observed that the drug loading raised steadily as the concentration of gellan was increased (Table 2) (Shelake et al., 2018). Further increase in gellan concentration above 2.4% caused a decline in drug loading capacity due to the gellan gums adsorption saturation on the GgE Nps surface. The maximum drug loading capacity of GgE NPs was found to be 960±0.9 mg at a 2.4% gellan concentration.

The *entrapment* efficiency of GgE nanoparticles increased with an increase in gellan concentration up to 2.4% (Table 2). Beyond 2.4%, *entrapment* efficiency decreased, which might be due to the drugs unavailability for *entrapment*. The entrapment efficiencies were higher for 2.4% gellan concentration (Nagarajan et al., 2015).

Table 2   Effect of gellan concentration on drug content and encapsulation efficiency

Gellan concentration (% w/v)	GgE NPs	
	Drug content (mg)	*EE%*
0.2	480±1.4	48±1.1
0.4	555.55±1.6	55±1.4
0.6	633.33±1.1	63±0.8
0.8	718.75±1.2	72±0.9
1.0	783.78±1.9	78±1.6
1.2	804.87±1.5	80±1.2
1.4	818.18±1.7	82±1.5

Table 2   Effect of gellan concentration on drug content and encapsulation efficiency (continued)

Gellan concentration (% w/v)	GgE NPs	
	Drug content (mg)	*EE%*
1.6	851.06±1.3	85±1.1
1.8	882.35±1.6	88±1.3
2	907.40±1.8	91±1.7
2.2	931.03±1.1	93±0.9
2.4	960±0.9	96±0.7

Table 3   Effect of drug concentration on drug content and entrapment efficiency

Drug concentration (% w/v)	GgE NPS	
	Drug content (mg)	*EE%*
0.2	105.26±1.4	53±0.9
0.4	241.75±1.7	60±1.3
0.6	419.75±1.2	70±0.8
0.8	600±1.6	75±1.2
1.0	800±1.1	80±0.8
1.2	983.05±1.3	82±1.1
1.4	1196.07±1.2	85±0.7
1.6	1422.22±1.6	89±1.4
1.8	1642.85±1.5	91±1.2
2	1846.15±1.8	92±1.5
2.2	2083.33±0.9	95±1.2
2.4	2357.14±1.9	98±1.6

3.5.9 *Effect of drug concentration on drug loading and entrapment efficiency*

From Table 3, it was found that as drug concentration was increased from 0.2% to 2.4% w/v, a sudden rise in drug loading from 105.26±1.4 mg to 2,357.14±1.9 mg was observed. However, a further increase in drug concentration might have led to a

saturation point, thereby lowering the drug loading capacity. The highest drug loading, $2{,}357.14\pm1.9$ mg of GgE NPs was attained when a 2.4% drug concentration was used. The % drug loading of GgE nanoparticles increased with increasing the concentration of drug and gellan polymer. Our results were in agreement with Masilamani and Ravichandiran (2012).

As the drug concentration increased from 0.2% to 2.4% w/v, entrapment efficiency increased (Table 3). The higher EE is because of the higher affinity of the drug and polymer in the same solvent. The *entrapment* efficiency declined with an increase in the concentration of erlotinib beyond 2.4%. The optimum entrapment efficiency was found to be 98% for 2.4% drug concentration. This finding was in agreement with Jawahar et al. (2009).

3.5.10 Effect of CaCl₂ concentration on drug loading and entrapment efficiency

Increasing the calcium chloride concentration from 0.1 to 1.0 M resulted in decreased drug loading and entrapment efficiency of GgE nanoparticles (Table 4). When calcium chloride concentration is increased, it leads to the non-solubilisation of drugs in the aqueous phase. Our results showed that rising $CaCl_2$ concentration (0.1 M) generated nanoparticles with greater levels of Ca^{2+} ions. As a result, the cross-linking of the gellan and compactness of the developed insoluble dense matrices also enhanced, resulting in higher drug entrapment in the nanoparticles. On the other hand, a further rise in $CaCl_2$ concentration above 0.1 M did not improve drug loading. This could be because of the potential saturation of calcium-binding sites in the gellan chain.

Table 4　Effect of calcium chloride concentration on drug content and entrapment efficiency

Calcium chloride concentration (M)	GgE NPs	
	Drug content (mg)	*EE%*
0.1	882.35±1.6	88±1.1
0.2	866.66±0.9	87±0.6
0.3	847.45±1.8	85±1.2
0.4	839.28±1.5	84±1.3
0.5	760±1.1	76±0.8
0.6	702.12±1.3	70±0.9
0.7	692.30±1.7	69±1.4
0.8	586.20±1.4	59±1.1
0.9	545.45±1.9	54±1.5
1.0	476.19±1.3	48±0.7

3.6 In-vitro drug release studies of GgE NPs

In-vitro drug release study was carried out using a dialysis bag technique. Figure 10 depicts the drug release profile of GgE NPs in citrate, carbonate bicarbonate and phosphate buffer. The release of erlotinib from the nanoparticles was investigated up to 1 h and 6 h to evaluate the controlled release potential of the developed GgE NPs. The release of erlotinib from the GgE NPs containing citrate buffer was found to be 86%, GgE NPs containing carbonate bicarbonate buffer recorded 78% and GgE NPs containing

phosphate buffer showed 81% of drug release after 1 hour. GgE NPs showed sustained drug release of 95% (acidic), 90% (neutral) and 83% (alkaline) at the end of 6 h. The erlotinib release was comparably faster at an acidic pH than at neutral or alkaline pH. The order of erlotinib release rate was citrate buffer (pH 4.8)> phosphate buffer (pH 7)> carbonate bicarbonate (pH 10.2). Among the three buffers used, acidic pH showed more sustained release than alkaline and neutral pH. These results were due to the increased solubility of erlotinib at an acidic pH. Thus polymeric nanoparticles could accurately and steadily release erlotinib, particularly in the acidic environment such as endolysosomes in tumor cells (Meng et al., 2014).

The *in-vitro* drug release pattern exhibited a burst release in the first 1 h accompanied by a controlled release of erlotinib for 6 h. The rapid drug release profile occurred from the nanoparticle in the initial stage because of the non-entrapped or loosely adhered drug was released on the nanoparticle surface. Erlotinib is a lipophilic compound and a weak base with a greater intestinal permeability. The free base is lightly soluble in water. The hydrochloride salt solubility is higher at a lower pH, showing the drug will readily dissolve in the acidic nature of the stomach. The primary release mechanism in encapsulated erlotinib from gellan gum is by diffusional processes through pores and the degradation of the polymeric network promotes the release. In contrast, the sustained release was attributed to the cleavage of the chemical bond between the drug and gellan gum.

Figure 10 *In-vitro* release of erlotinib-loaded gellan gum nanoparticles observed at (A) 1 h (b) 6 h (see online version for colours)
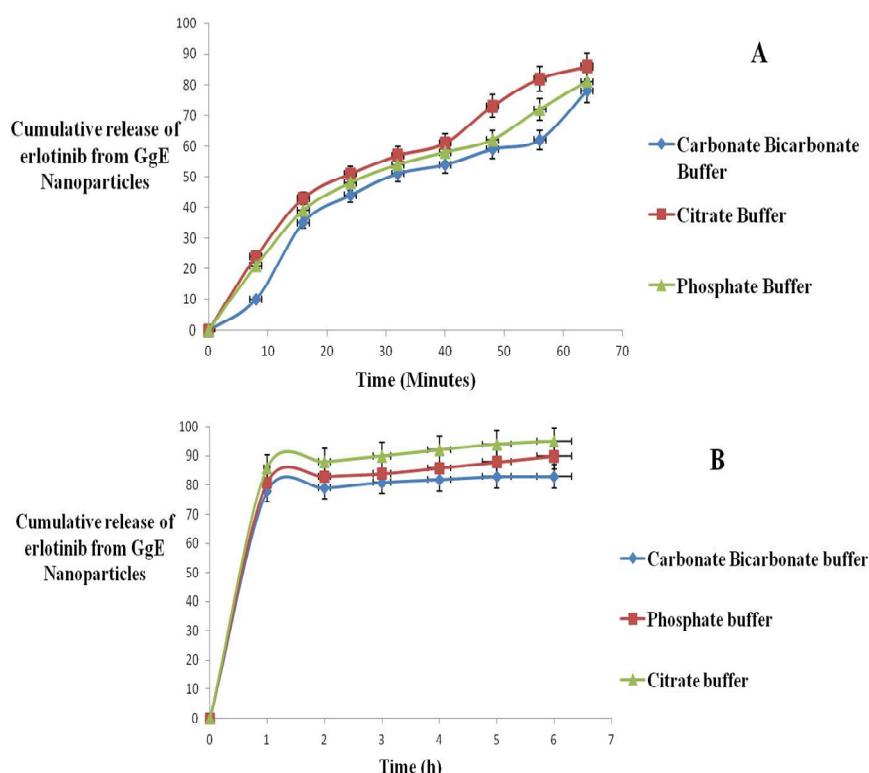
3.7 SRB assay results

The inhibitory effect of gellan gum, erlotinib and GgE NPs was evaluated against HepG2 cancer cell lines at different concentrations (5, 10, 20, 40, 80 and 100 μm). The percentage inhibition of proliferation of cells at different concentrations of gellan gum, erlotinib and GgE NPs was calculated based on the formula:

%   Inhibition of proliferation

=   100-{(Mean OD of treated sample-mean OD of zero control)

/   (Mean OD control-mean OD of zero control)}*100.

Figure 11 Cytotoxic effect of gellan gum, erlotinib and GgE NPs against HepG2 cell line by SRB assay (see online version for colours)
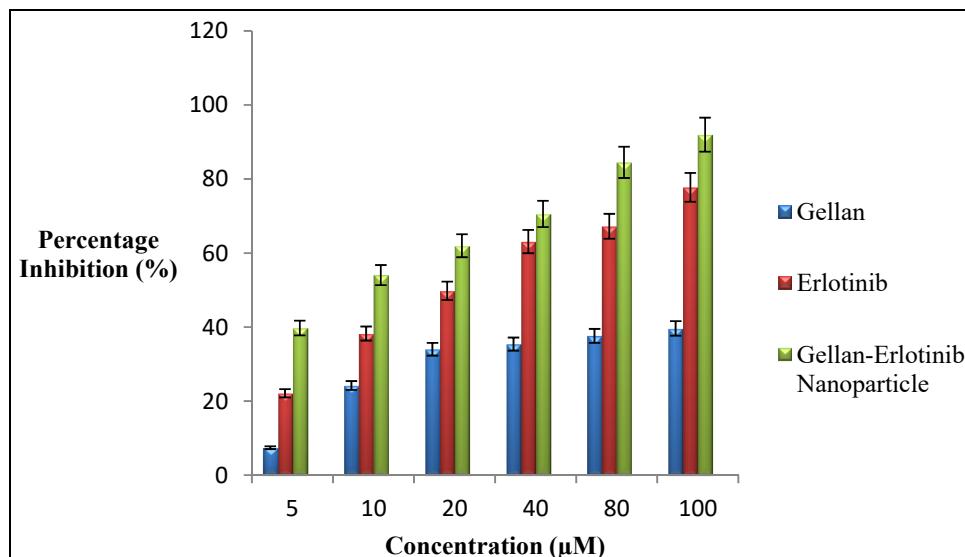
The concentration and percentage inhibition curve after 48 h incubation with gellan gum, erlotinib and GgE NPs are illustrated in Figure 11. As the concentration of GgE NPs increases, it was observed that there was a significant increase in cell toxicity, reducing the cell count from 40% (5 μm) to 92% (100 μm). However, in gellan gum and erlotinib, there was not much significant decrease in total cell number. In the case of erlotinib, cell count decreased from 22% (5 μm) to 78% (100 μm), whereas in gellan gum, cell count accounts for 7.4% (5 μm) to 40% (100 μm). The results suggest that GgE NPs showed potent cytotoxicity against the HepG2 cell line in a concentration-dependent manner among the samples. The IC_{50} values for gellan gum, erlotinib and GgE NPs against HepG2 cell line were calculated to have a better insight. The IC_{50} value was found to be 99.2 μM for gellan gum, 53.9 μM for erlotinib and 44.6 μM for GgE NPs. Thus it was concluded that erlotinib-loaded gellan gum nanoparticles exhibited the highest *in-vitro* anticancer activity than free erlotinib and gellan gum as supported by the IC_{50} value (Jaya Prakash et al., 2014).

Gellan gum is inert in biological systems and does not influence cell viability. It has been reported that the gellan gum is biocompatible with various types of cells. SRB

results showed the pivotal role of NPs binding and internalisation in improving cytotoxic activity. In the cell cytotoxicity assay, gellan gum did not significantly influence the viability of HepG2 cells. These results indicated gellan itself did not influence the proliferation of tumor cells. Hence, the interference of the carrier itself was negligible in this study.

4   Conclusions

The erlotinib-loaded gellan gum nanoparticles were synthesised by the emulsion cross-linking method and calcium chloride solution was used as the cross-linking agent. The morphology of the GgE nanoparticles was investigated by SEM. The FTIR results showed the interaction between polymer and drug. DSC, TGA and XRD measurements exhibited the ability of the nanoparticles to encapsulate the drug successfully. Nanoparticles showed an average particle size of 655 nm and exhibited narrow distribution with a polydispersity index of 0.49. The surface charge of the nanoparticles was confirmed by zeta potential. Drug loading and entrapment efficiency of GgE NPs were influenced by the gellan and erlotinib concentration. When the concentration of gellan and drug was increased, drug loading was found to be improved. GgE NPs exhibited the highest entrapment efficiency at 2.4% gellan concentration. The dialysis method was carried out to study *in-vitro* drug release. The erlotinib release from GgE NPs was about 86%, 81% and 78% for pH 4.8, pH 7 and pH 10.2 respectively. *In-vitro* drug release study indicated a faster release in acidic buffer compared to neutral and alkaline. The IC_{50} values for GgE NPs, erlotinib and gellan gum in HepG2 cells after 48h of incubation were 44.6 µM, 53.9 µM and 99.2 µM respectively. The SRB assay results revealed that the GgE NPs exhibited potent cytotoxicity against the HepG2 cell line. Ease of production under mild preparation conditions, higher levels of drug encapsulation and desirable biocompatibility are the benefits of the erlotinib-loaded gellan gum nanoparticles. The sustained release of erlotinib from the GgE NPs showed that biodegradable polymeric nanoparticles could be a promising drug carrier for anticancer drugs.

References

Bajaj, I.B., Survase, S.A., Saudagar, P.S. and Singhal, R.S. (2007) 'Gellan gum: fermentative production, downstream processing and applications', *Food Technol Biotech*, Vol. 45, No. 4, pp.41–354.

Bera,H., Abbasi ,Y.F., Lee, P. L., Marbaniang, D., Mazumder, B., Kumar, P., Tambe, P., Gajbhiye, V., Cun, D. andYang, M. (2020) 'Erlotinib-loaded carboxymethyl temarind gum semi-interpenetrating nanocomposites', *Carbohydr Polym*, Vol. 230, p.115664.

Das, S., Banerje, R. and Belare, J. (2005) 'Aspirin loaded albumin nanoparticles by coacervation: implications in drug delivery', *Trends BiomaterArtif Organs*, Vol. 18, No. 2, pp.203–212.

Dhar, S., Murawala, P., Shiras, A., Pokharkar, V. and Prasad, B.L.V.(2012) 'Gellan gum capped silver nanoparticle dispersions and hydrogels: cytotoxicity and in vitro diffusion studies', *Nanoscale*, Vol. 4, No. 2, pp.563–567.

Fialho, A.M., Maitins, L.O., Donval, M.L., Leitato, J.H., Ridout, M.J., Jay, A.J., Morris, V.J. and Correia, Isa. (1999) 'Structures and properties of gellan polymers produced by Sphingomonas paucimobilis ATCC 31461 from lactose compared with those produced from glucose and from cheese whey', *Appl Environ Microbiol*, Vol. 65, No. 6, pp.2485–2491.

Govender, T., Stolnik, S., Garnett, M.C., Illum, L. and Davis, S.S. (1999) 'PLGA nanoparticles prepared by nanoprecipitation: drug loading and release studies of a water soluble drug', *J. Controlled Release*, Vol. 57, No. 2, pp.171–85.

Gültekin, H. and Değim, Z. (2013) 'Biodegradable polymeric nanoparticles are effective systems for controlled drug delivery', *FABAD J. Pharm. Sci.*, Vol. 38, No. 2, pp.107–118.

Güncüm, E., Işıklan, N., Anlaş, C., Ünal, N., Bulut, E., Bakırel, T. (2018) 'Development and characterization of polymeric-based nanoparticles for sustained release of amoxicillin – an antimicrobial drug', *Artif Cells Nanomed Biotechnol.*, Vol. 46, No. 2, pp.964–973.

Heller, J. and Domb, A.J. (2003) 'Recent developments with biodegradable polymers', *Adv, Drug Deliver Rev,*, Vol. 55, No. 4, pp.445–446.

Jawahar, N., Nagasamy, V.D., Sureshkumar, R., Senthil, V., Ganesh, G.N.K., Vinoth, P., Sumeet, S. and Samanta, M.K. (2009) 'Development and characterization of PLGA-nanoparticles containing carvedilol', *J. Pharm. Sci. Res.*, Vol. 1, No. 3, pp.123–128.

Jaya Prakash, S., Santhiagu, A. and Jasemine, S. (2014) 'Preparation, characterization and in vitro evaluation of novel gellan gum-raloxifene HCl nanoparticles', *Journal of Pharmaceutical and Biosciences*, Vol. 2, pp.63–71.

Jeong ,Y.I., Jin, S.G., Kim, I.Y., Pei ,J., Wen, M., Jung, T.Y., Moon, K.S. and Jung, S. (2010) 'Doxorubicin-incorporated nanoparticles composed of poly(ethylene glycol)-grafted carboxymethyl chitosan and antitumor activity against glioma cells in vitro', *Colloids Surf Biointerfaces*, Vol. 79, No. 1, pp.149–155.

Katiyar, S., Pandit, J., Mondal, R.S., Mishra, A.K., Chuttani, K., Aqil, M., Ali, A. and Sultana, Y. (2014) 'In situ gelling dorzolamide loaded chitosan nanoparticles for the treatment of glaucoma', *Carbohydr Polym*, Vol. 15, No. 102, pp.117–124.

Kumar, S., Dilbaghi, N., Saharan, R. and Bhanjana, G. (2012) 'Nanotechnology as emerging tool for enhancing solubility of poorly water-soluble drugs', *Bio Nano Sci.*, Vol. 2, pp.227–50.

Lu, Y., Zhao, X. and Fang, S. (2019) 'Characterization, antimicrobial properties and coatings application of gellan gum oxidized with hydrogen peroxide', *Foods*, Vol. 8, No. 1, p.31.

Mahapatro, A.and Singh, D.K. (2011) 'Biodegradable nanoparticles are excellent vehicle for site directed in-vivo delivery of drugs and vaccines', *Journal of Nanobiotechnology*, Vol. 9, No. 28, p.55.

Mahesh, D.C., Khdair, A., Patil, Y., Handa, H., Mao, G. and Jayanth, P. (2007) 'Polymer-surfactant nanoparticles for sustained release of water-soluble drugs', *J. Pharm. Sci.*, Vol. 96, No. 12, pp.3379–3389.

Masilamani, K. and Ravichandiran, V. (2012) 'Effect of formulation and process variables on drug content and entrapment efficiency of aceclofenac nanosuspension', *Materials Science*, Vol. 3, No. 3, pp.315–318.

Meng, F., Zhong, Y., Cheng, R., Deng, C. and Zhong, Z. (2014) 'pH-sensitive polymeric nanoparticles for tumor-targeting doxorubicin delivery: concept and recent advances', *Nanomedicine*, Vol. 9, No. 3, pp.487–499.

Nagarajan, E., Shanmugasundaram, P., Ravichandirana, V., Vijayalakshmi, A., Senthilnathan, B. and Masilamani, K. (2015) 'Development and evaluation of chitosan based polymeric nanoparticles of an antiulcer drug lansoprazole', *J. App. Pharm. Sci.*, Vol. 5, No. 4, pp.20–25.

Panyam, J. and Labhasetwar, V. (2003) 'Biodegradable nanoparticles for drug and gene delivery to cells and tissue', *Adv. Drug Del. Rev.*, Vol. 55, No. 3, pp.329–347.

Sailaja, A., Amareshwar, P. and Chakravarty, P. (2011) 'Different techniques used for the preparation of nanoparticles using natural polymers and their application', *Int. J. Pharm. Sci.*, Vol. 3, No. 2, pp.45–50.

Sharma, S., Parmar, A., Kori, S. and Sandhir, R. (2016) 'PLGA-based nanoparticles: a new paradigm in biomedical applications', *Trends Anal. Chem.*, Vol. 80, pp.30–40.

Shelake, S., Patil, S., Patil, S. and Sangave, S. (2018) 'Formulation and evaluation of fenofibrate-loaded nanoparticles by precipitation method', *Indian J. Pharm. Sci.*, Vol. 80, No. 3, pp.420–427.

Singh, G., Faruk, A. and Bedi, P.M.S. (2018)'Spectral analysis of drug loaded nanoparticles for drug-polymer interactions', *Journal of Drug Delivery and Therapeutics*, Vol.8, No. 6, pp.111–118.

Singh, R. and Lillard Jr., J.W. (2009) 'Nanoparticle-based targeted drug delivery', *Experimental and Molecular Pathology*, Vol. 86, No. 3, pp.215–223.

Skehan, P., Storeng, R., Scudiero, D., Monks, A., McMahon, J., Vistica, D., Warren, J.T., Bokesch, H., Kenney, S. and Boyd, M.R. (1990) 'New colorimetric cytotoxicity assay for anticancer-drug screening', *J. Natl. Cancer Inst.*, Vol. 82, No. 13, pp.1107–1112.

Soppimath, K.S., Aminabhavi, T.M., Kulkarni, A.R. and Rudzinski, W.E. (2001) 'Biodegradable polymeric nanoparticles as drug delivery devices', *J. Control Release*, Vol. 70, NoS.1–2, pp.1–20.

Soumiya, S., Santhiagu, A. and Manjusha, C.M. (2021) 'Cloning of gellan gum biosynthetic genes gelC, gelD and gelE for enhanced production of gellan gum by Sphingomonas paucimobilis ATCC 31461', *Res. J. Biotech*, Vol. 16, No. 2, pp.133–140.

Sun, S.B., Liu, P., Shao, F.M. and Miao, Q.L. (2015) 'Formulation and evaluation of PLGA nanoparticles loaded capecitabine for prostate cancer', *International Journal of Clinical and Experimental Medicine*, Vol. 8, No. 10, pp.19670–19681.

Unsoy, G., Khodadust, R., Yalcin, S., Mutlu, P. and Gunduz, U. (2014) 'Synthesis of Doxorubicin loaded magnetic chitosan nanoparticles for pH responsive targeted drug delivery', *Eur. J. Pharm. Sc.i*, Vol. 62, No. 1, pp.243–50.

Varsha, P., Vikram, P. and Leenata, M. (2015)'Engineering of polymer–surfactant nanoparticles of doxycycline hydrochloride for ocular drug delivery', *Drug Delivery*, Vol. 22, No. 7, pp.955–968.